

The role of atomic interactions in cavity-induced continuous time crystals

Christian H. Johansen¹, Johannes Lang^{1,2}, Francesco Piazza^{1,3*}

¹ Max-Planck-Institut für Physik komplexer Systeme, 01187 Dresden, Germany

² Institut für Theoretische Physik, Universität zu Köln, Zùlpicher Straße 77, 50937 Cologne, Germany

³ Theoretical Physics III, Center for Electronic Correlations and Magnetism, Institute of Physics, University of Augsburg, 86135 Augsburg, Germany

* francesco.piazza@uni-a.de

November 12, 2023

1 Abstract

We consider continuous time-crystalline phases in dissipative many-body systems of atoms in cavities, focusing on the role of short-range interatomic interactions. First, we show that the latter can alter the nature of the time crystal by changing the type of the underlying critical bifurcation. Second, we characterize the heating mechanism and dynamics resulting from the short-range interactions and demonstrate that they make the time crystal inherently metastable. We argue that this is generic for the broader class of dissipative time crystals in atom-cavity systems whenever the cavity loss rate is comparable to the atomic recoil energy. We observe that such a scenario for heating resembles the one proposed for preheating of the early universe, where the oscillating coherent inflation field decays into a cascade of exponentially growing fluctuations. By extending approaches for dissipative dynamical systems to our many-body problem, we obtain analytical predictions for the parameters describing the phase transition and the heating rate inside the time-crystalline phase. We underpin and extend the analytical predictions of the heating rates with numerical simulations.

1 Introduction

Following the first conceptualization of time-crystalline phases of matter [1, 2], it was quickly proven that such phases cannot appear in thermal equilibrium [3–5]. However, it turned out to be possible to realize such phases in periodically driven systems, both closed [6–11] and dissipative [12, 13].

Among the latter, systems of atoms in optical cavities have emerged as an ideal platform to realize continuous time-crystalline phases [14–16], where an effectively time-independent drive of the atomic system is counterbalanced by the loss of photons out of the cavity mirrors. In these phases, continuous time-translation invariance is spontaneously broken, and oscillations persist even though the system possesses a macroscopic number of degrees of freedom, among which energy can be redistributed via interactions.

Since the phase space of scattering by cavity-mediated interactions between atoms is limited, due to their long range, redistribution of energy through these processes is inefficient [17–19]. However, the intrinsic atomic short-range interactions allow for efficient redistribution of energy among the atoms. Indeed, experiments show strong indications

33 that these interactions are one of the main fundamental limiting factors to the measured
 34 lifetime of the time crystal [12].

35 Despite their crucial role short-range atomic interactions have not been theoretically
 36 investigated so far in a systematic way for continuous time crystals in atom-cavity setups.
 37 In this work, we undertake this task. Not only do we provide a full picture of the possible
 38 destabilization processes but we also show that short-range interactions can alter the
 39 nature of the time crystal itself.

40 We consider a simple and experimentally realizable mechanism for the appearance of
 41 time-crystalline phases for an interacting BEC coupled to two cavity modes [20]. By ex-
 42 tending approaches for classical non-linear dissipative systems to our many-body problem,
 43 we obtain an analytical description of the time crystal in terms of cavity-induced critical
 44 bifurcations and show how inter-atomic interactions can modify the nature of the latter.
 45 Within this approach, we also compute the dependence of the energy-redistribution rates
 46 on external parameters and identify the scattering processes responsible for making the
 47 time crystal metastable.

48 The analytical understanding of the results, which we also underpin with numerical
 49 analysis, allows for a deep insight into the generic features of the phenomenology beyond
 50 the specific model considered and provides orientation for future investigations both in
 51 theory and experiment.

52 2 Model

53 The system considered is an ultracold gas of bosonic atoms in a BEC state, dispersively
 54 coupled with equal strength to two modes of an optical cavity. In this regime, a photon
 55 imparts a recoil momentum of $Q = 2\pi/\lambda$ to an atom, with λ being the wavelength of
 56 the photon in a given mode. In the thermodynamic limit, the atomic BEC at momentum
 57 k is described by a complex field ψ_k satisfying the Gross-Pitaevski mean-field equations.
 58 Furthermore, in the limit of a small transverse extend of the BEC compared to the cavity
 59 waist we can simplify the model to one spatial dimension [19, 20]

$$i\partial_t\psi_k = k^2\psi_k + U \sum_{q,q'} \psi_q\psi_{q'}\bar{\psi}_{q+q'-k} + \frac{\tilde{\eta}}{\sqrt{2}} \sum_{j=1,2} \text{Re}(\phi_j) (\psi_{k+Q} + \psi_{k-Q}), \quad (1)$$

60 where the bar denotes complex conjugation. This equation has been written in units of the
 61 recoil energy $E_R = \hbar^2 Q^2/2m$ and in the rotating frame of the laser. The time-dependence
 62 of the fields is kept implicit and the atom field has been normalized to 1. The cavity-mode
 63 wavelengths have been chosen to be equal, as we assume the modes differ in the transverse
 64 direction [20]. The coupling strength $\tilde{\eta}$ can experimentally be tuned by the strength of
 65 the transverse pump while the atoms are interacting with each other through a contact
 66 interaction of strength U . The complex field ϕ_j corresponds to the coherent cavity-field
 67 amplitude which satisfies the equation

$$i\partial_t\phi_j = (\Delta_j - i\kappa)\phi_j + \frac{\tilde{\eta}}{2\sqrt{2}} \sum_{k=-\infty}^{\infty} \bar{\psi}_k (\psi_{k+Q} + \psi_{k-Q}), \quad (2)$$

68 where the cavity field has been normalized by the square root of the atom number. The
 69 cavity linewidths, κ , have been assumed to be identical for both modes. In the following we
 70 will consider κ on an energy scale similar to the recoil energy, as realized for instance in [21].
 71 In the actual implementation of the dispersive atom-cavity coupling, the characteristic
 72 frequency of each cavity mode Δ_j corresponds to the detuning of the mode frequency

73 with respect to laser-driven two-photon transitions [20]. The steady-state of this model
 74 can break time-translation invariance when the two detunings have opposite signs. With
 75 this in mind the detunings are parametrized as $\Delta_1 = -(\Delta - \frac{\delta}{2})$ and $\Delta_2 = \Delta + \frac{\delta}{2}$. By
 76 choosing $0 < \delta < 2\Delta$ the negative detuning has the smallest amplitude $|\Delta_1| < |\Delta_2|$.

77 3 Nature of the time crystal

78 Below a critical coupling strength η_c , all atoms are in the homogeneous state ψ_0 , and the
 79 coherent part of the cavity fields is empty. This configuration is denoted as the normal
 80 phase (NP) and it is always a fixed point of the equations of motion Eqs. (1) and (2).
 81 As $\tilde{\eta}$ is increased beyond η_c the NP fixed point becomes unstable and the system enters
 82 a state where a fraction of the atom population is transferred to $\psi_{\pm Q}$ and the coherent
 83 fields of the cavity becomes finite. This symmetry-broken state is often referred to as
 84 the superradiant (SR) or self-organized state [22, 23]. The frequency ω_c of the excitation
 85 becoming undamped above η_c , can be derived through a linear expansion around the NP
 86 fixed point [24] (see [25] for an alternative approach). One finds three non-negative real
 87 solutions for the frequency of the critical mode. These three solutions are $\omega_c = 0$, a
 88 resonance at the energy of the Bogoliubov excitation of the BEC at the recoil momentum
 89 $\omega_c = \omega_a = \sqrt{E_R(E_R + 2U)}$ and a solution given by

$$\omega_c = \sqrt{\frac{\delta^2}{4} + \sqrt{(4\Delta^2 - \delta^2)(\Delta^2 + \kappa^2)} - \Delta^2 - \kappa^2}, \quad (3)$$

90 which is solely determined by cavity parameters, that is, it does not depend on U and E_R .
 91 This feature, which can be attributed to the fact that the cavity is the only dissipation
 92 channel, implies a robustness of this self-sustained periodic signal to perturbations of the
 93 nonlinear medium that causes this signal to appear in the first place. Out of the three
 94 modes the critical one is identified by having the smallest real critical coupling. Differently
 95 from the frequency, the critical coupling given by

$$\eta_c = \sqrt{\frac{\omega_a^2 - \omega_c^2}{E_R \sum_{j=1,2} \frac{\Delta_j(\Delta_j^2 + \kappa^2 - \omega_c^2)}{\omega_c^4 + 2\omega_c^2(\kappa^2 - \Delta_j^2) + (\Delta_j^2 + \kappa^2)^2}}}, \quad (4)$$

96 always depends on both cavity and atom parameters [24]. The phase diagram will therefore
 97 depend on all parameters of the theory.

98 In Fig. 1(a) the frequency of the critical mode at η_c is plotted as a function of κ and Δ
 99 and is a good order parameter for distinguishing the three different phases of the system.
 100 For $\Delta < \delta/2$ both cavity modes have a positive detuning and the system always exhibits
 101 static superradiance (SSR), characterized by a critical mode with zero frequency. SSR
 102 requires a finite critical atom-cavity coupling such that the critical mode is a polariton.
 103 For $\Delta > \delta/2$ one of the modes acquires a negative detuning. Differently from a positively-
 104 detuned mode, a negatively-detuned one disfavors a superradiant density modulation.
 105 The competition between the two cavity modes induces an oscillating superradiant phase
 106 (OSR) [20, 26], which also requires a finite coupling strength such that the critical mode
 107 is again a polariton. Instead, when ω_c equals ω_a , the critical coupling η_c in Eq. (4)
 108 vanishes, making the critical mode purely atomic. We refer to this instability as the
 109 atomic instability (AI).

110 Both the OSR and AI critical modes break continuous time-translation invariance and
 111 can thus potentially signal a continuous time-crystal phase. However, whether the latter

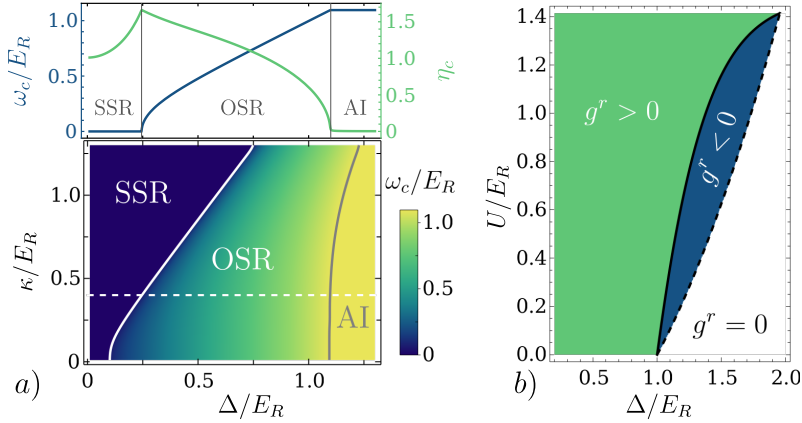


Figure 1: The critical frequency of the instability is shown in the lower plot of a) as a function of Δ and κ . By tuning Δ the critical mode change from exhibiting static to oscillating superradiance and a purely atomic instability over a large range of cavity loss rates. Above the critical frequency and coupling is shown along the white dashed line. The upper plot shows the critical frequency and coupling along the dashed line in the lower plot. In b) the sign of the cubic interaction as a function of Δ and U is plotted for $\kappa = 0.4E_R$. This determines the stability of the symmetry-broken state beyond the linear analysis. For the entire figure $\delta = 0.2E_R$.

112 is stable is determined by non-linear effects not included so far. In order to capture
 113 these in the present interacting many-body system, we perform a systematic perturbative
 114 expansion in the relative distance from the critical point $\eta = (\tilde{\eta} - \eta_c) / \eta_c$. The resulting
 115 effective non-linear equation is of the Stuart-Landau form (see e.g. [27]), and is an equation
 116 of motion for the collective degrees of freedom which are excited in the SR phases. These
 117 degrees of freedom constitute the so-called center manifold and are defined by the critical
 118 mode, which is composed of both cavity modes as well as of the zero and recoil momentum
 119 components of the BEC, ψ_0 and $\psi_{\pm Q}$. Within the center manifold and to leading order in
 120 η the recoil momentum component is given by

$$\psi_{\pm Q}(t) = \sqrt{\eta}R (c_+ e^{i\omega_c t} + c_- e^{-i\omega_c t}), \quad (5)$$

121 with c_{\pm} being the atomic components of the critical-mode eigenvector obtained from the
 122 linear analysis [24]. The cavity fields have the same form with c_{\pm} replaced by the cavity
 123 components of the critical mode. Finally, since to leading order the only occupied atom
 124 components are ψ_0 and $\psi_{\pm Q}$, these are linked by normalization such that

$$\psi_0 = \sqrt{1 - |\psi_Q|^2 - |\psi_{-Q}|^2} \sim b_0 + b_+ e^{i2\omega_c t} + \bar{b}_+ e^{-i2\omega_c t}, \quad (6)$$

125 with $b_0 = 1 - \eta R^2 (|c_+|^2 + |c_-|^2)$ and $b_+ = -\eta R^2 c_+ \bar{c}_-$. The perturbative approach yields
 126 an equation of motion for the amplitude, R , in the symmetry-broken phase:

$$\dot{R} = \gamma R - g^r R^3, \quad (7)$$

127 where γ is the exponential growth rate of the critical mode obtained from the linear
 128 analysis, which in this case can be shown to be positive. The non-linearity of the center
 129 manifold or in other words, the strength of the self-interaction of the excitations present
 130 in the critical mode, is quantified by g^r (see Appendix A.2 for closed expressions for these

131 quantities and the proof of the sign of γ). For stable time-crystalline and static solutions,
 132 R must be time-independent, real, and positive:

$$R = \sqrt{\frac{\gamma}{g^r}} > 0. \quad (8)$$

133 As $\gamma > 0$, our analytic solutions can only be stable if $g^r > 0$. This is physically clear since
 134 otherwise the attractive self-interaction would lead to a first order transition into a phase
 135 that requires higher-order non-linearities for stabilization.

136 The sign of g^r is shown in Fig. 1(b). If ω_c is pushed to ω_a , $g_r = 0$ i.e. the self-interaction
 137 vanishes as the critical mode is purely atomic, which corresponds to the white region in
 138 Fig. 1(b). As the fraction γ/g^r goes to zero as ω_c approaches ω_a (see Eq. (31)), the AI
 139 phase has no stable time-crystalline solution.

140 Short-range interactions between the atoms qualitatively modify g^r and lead to two
 141 separatrices in Fig. 1(b). The expression for the separatrix $U_{c2}(\Delta)$, drawn with a solid line
 142 is given in Eq. (27), while the separatrix $U_{c1}(\Delta)$ between the white and the blue region,
 143 is defined by the condition that the energy cost of a Bogoliubov excitation, ω_a , equals Δ .
 144 When $U > U_{c1}$ the self-interactions of the critical mode become finite and repulsive as
 145 $\omega_c < \omega_a$, leading to a finite cavity component of the critical mode.

146 It is further remarkable that the sign of the self-interactions can be changed via U .
 147 Indeed, within the blue region in Fig. 1(b), that is, for $U_{c1} < U < U_{c2}$, the self-interactions
 148 of the critical mode are attractive: $g_r < 0$. This is due to the fact the short-range
 149 repulsion U , which penalizes density modulations and in particular excitation of the recoil
 150 component $\psi_{\pm Q}$, is not sufficient to counteract the decrease of energy due to coupling
 151 to the negatively detuned cavity mode. The resulting instability of the stationary OSR
 152 solution corresponds to a subcritical Hopf bifurcation [28] of Eq. (6). On the other hand,
 153 when $U > U_{c2}$ (green region in the figure), the short-range repulsion penalizes density-
 154 modulations enough to change the sign of the self-interaction of the critical mode and
 155 thus stabilize the OSR phase. This corresponds to a transition from a subcritical to a
 156 supercritical Hopf bifurcation.

157 4 Energy redistribution and melting of the time crystal

158 The OSR time crystal is thus, up to this point, found to exist in a stable fashion as a
 159 supercritical Hopf bifurcation. Still, to fully assess its stability, one must allow for energy
 160 redistribution between all degrees of freedom, including those not belonging to the critical
 161 polariton mode defining the center manifold of the bifurcation. We will refer to those as
 162 the not-center-manifold (NCM) modes. Hence, one needs to treat the many-body problem
 163 of scattering between quasi-particles and a time-dependent coherent field.

164 Let us first predict which NCM modes initially participate in the scattering process,
 165 assuming we are only slightly into the OSR phase. In this regime, we can exploit our
 166 analytical knowledge from Eqs. (5) and (6). The fastest-growing NCM mode results from
 167 scattering between the atomic components b_0 and c_{\pm} of the center manifold, as illustrated
 168 in Fig. 2(a). For this process, the outgoing NCM modes with energies $\epsilon_q, \epsilon_{q'}$ have to
 169 satisfy $q + q' = Q$, $\epsilon_q + \epsilon_{q'} = \omega_c$. Since here $q \neq -q'$, we call this the asymmetric channel.
 170 Near the critical point, we can approximate ϵ_q with the Bogoliubov dispersion of the BEC
 171 excitations in the absence of the cavity field, which for small U reads $\omega_B(k) \approx E_R k^2 + U$.
 172 This yields $q = Q/2 + \sqrt{\omega_c - E_R/2 - 2U}/\sqrt{2}$ and $q' = Q - q$. From the approximation
 173 of the CM components in Eqs. (5) and (6), we predict an exponential growth of these
 174 two Bogoliubov modes with a rate Γ that is proportional to $U\sqrt{\eta}$. This asymmetric

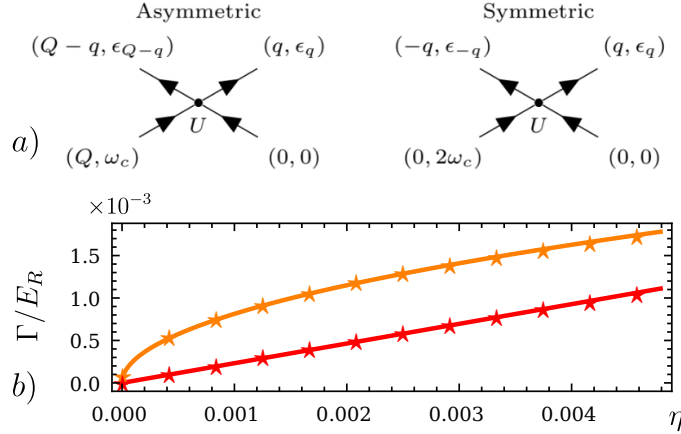


Figure 2: a) The dynamic nature of the OSR phases combined with finite atom-interaction leads to occupation of atom modes out of the center manifold, through the symmetric and asymmetric process illustrated here. b) The scaling of the growth rates, computed from the Floquet quasi-energies of the linearized equations, for the asymmetric channel marked with orange stars, with a square-root fit (orange line) and the scaling of symmetric channel marked with red stars, with a linear fit (red line). The same parameters as in Fig. 3 have been used.

175 channel can be closed off if $\omega_c < E_R/2 - 2U$, which leaves us with a different channel
 176 where the component b_0 scatters with b_+ , or c_+ with c_- . Both these processes produce
 177 a symmetric NCM pair with $q = -q' = \sqrt{\omega_c - U}$. One representative process of this
 178 symmetric channel is shown in Fig. 2(a). In contrast to the asymmetric counterpart, we
 179 predict Γ to be proportional to $U\eta$ for the symmetric scattering processes.

180 In order to further verify the above predictions, we have linearized Eqs. (1) and (2)
 181 around the OSR phase and extracted the rate by computing the Floquet quasi-energies.
 182 The details of these calculations can be found in Appendix B and the resulting growth rates
 183 are shown in the lower panel of Fig. 3. It is seen that the predicted momentum (orange
 184 marks for the asymmetric channel and red mark for the symmetric channel) is only reliable
 185 close to the phase transition as the dispersion of the NCM mode is quickly modified due
 186 to the growing oscillating density modulation. We also find an additional momentum
 187 component that grows (marked in green), which arises from the scattering between a
 188 negative momentum NCM mode in the symmetric channel and the recoil component of the
 189 center manifold. The computed growth rates for the symmetric and asymmetric modes are
 190 shown in Fig. 2(b), and in both cases, an excellent agreement with our simple predictions
 191 based on Fig. 2(a) is demonstrated. Finally, in order to fully confirm our predictions,
 192 we performed a full numerical integration using a Runge-Kutta-4 routine, starting from
 193 the OSR phase at $\eta = 0.06$, corresponding to the white dashed line in the lower panel of
 194 Fig. 3. After evolving the system for 200 periods we compared the momentum distribution
 195 with the predictions based on the Floquet quasi-energies and found excellent agreement,
 196 as shown in the upper panel of Fig. 3.

197 An important outcome of our analysis is that the time crystal in these systems always
 198 have a finite lifetime due to the energy redistribution caused by scattering out of the
 199 center manifold. Its lifetime, however, increases significantly by considering $\omega_c < E_R/2$
 200 to prohibit the asymmetric scattering processes that lead to much higher growth rates.
 201 As interatomic interactions can be weak in dilute systems, the time crystalline phases can
 202 appear stable on a long time scale making them metastable.

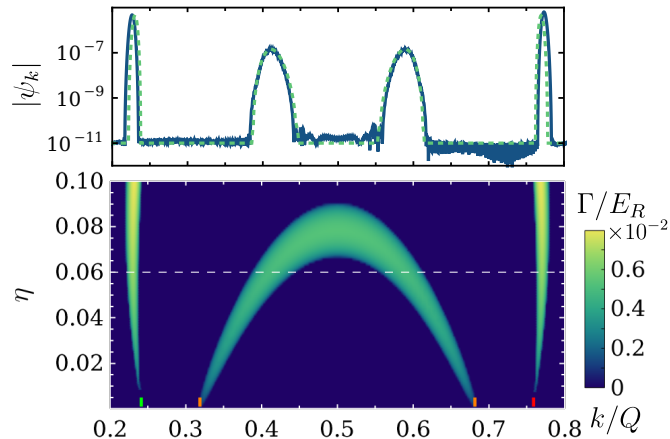


Figure 3: The lower plot shows the exponential growth rates of the atomic modes outside of the center manifold. The parameters are equivalent to those in Fig. 1 with $\Delta = 0.6E_R$ resulting in $\omega_c = 0.586E_R$, and we choose $U = 0.01E_R$. The orange ticks indicate the predicted momentum based on the asymmetric channel, while the red tick signifies the symmetric channel momentum. The green tick is the atom mode coupled to the symmetric channel through the cavity. The upper plot shows the resulting atom distribution after 200 periods at the dashed line in the lower plot, both with numerical integration of Eqs. (1) and (2) in blue and from the linearized prediction with the dashed green line.

203 5 Conclusion

204 We have provided a systematic analysis of the role of short-range interactions on the nature
 205 and stability of continuous time crystals in dissipative many-body systems of ultracold
 206 bosonic atoms in cavities.

207 First, we have shown that short-range interatomic interactions can alter the nature of
 208 the time crystal by transforming the underlying classical bifurcation from sub- to super-
 209 critical.

210 Second, we have studied the effect of short-range interactions on heating and melting
 211 of the time crystal. The heating mechanism we have discussed arises due to the oscillating
 212 nature of the atomic fields ψ_0 and $\psi_{|Q|}$. As shown in Eq. (35), the amplitude of these
 213 fields is not dependent on the details of the underlying critical polaritonic mode, but only
 214 depend on the frequency of the oscillations and the proper dimensionless distance from
 215 the critical point.

216 Furthermore, we find that the cavity losses cannot efficiently cool the system [29–31]
 217 (NCM modes can be de-excited only at higher order in our expansion, see Appendix B).
 218 This suggests that the heating mechanism we identified is generic for these cavity systems
 219 [32], as long as the cavity line width is comparable to the recoil energy. We note that time-
 220 dependent Hartree-Fock approximations would miss this heating [33], as they lack collisions
 221 and thus redistribution [34]. As we show it is precisely these effects that eventually lead to
 222 the metastable nature of the time-crystalline state, consistent with numerical predictions
 223 in related models [35, 36].

224 Finally, we point out that the heating mechanism described here is analogous to pre-
 225 heating in the early universe [37, 38], where the weakly interacting and oscillating, co-
 226 herent inflation field decays into a cascade of exponentially growing fluctuations, leading
 227 to extreme non-equilibrium conditions inaccessible to perturbative methods and finally

228 to prethermalization [39]. The analytic discussion presented here corresponds to the lin-
 229 earized classical regime [40], which at later times will be superseded by increasingly non-
 230 linear effects leading to a cascade of even more quickly growing fluctuations that eventually
 231 thermalize [41] and thus destroy the time-crystalline phase. It will be interesting to pur-
 232 sue this analogy deeper into the highly excited regime using appropriate atom-photon
 233 diagrammatic approaches [42, 43].

234 Acknowledgements

235 CHJ would like to thank Johnathan Dubois for many helpful and insightful discussions.

236 A Center manifold coefficients

237 The two-cavity mode system considered is a simplification of the N cavity mode system
 238 discussed in [24]. This thesis contains a detailed analysis of the origin of the limit cycle,
 239 which we use as foundation for our exploration.

240 The starting point is the equations of motion in Eqs. (1) and (2), which we use to
 241 define the autonomous system of non-linear first order ODE's

$$\dot{\mathbf{v}} = F(\mathbf{v}), \quad (9)$$

242 Here \mathbf{v} is a vector containing the two complex cavity fields and all the complex atom
 243 fields with the different discretized momenta. As both cavity modes transfer the same
 244 longitudinal momentum (Q) and the BEC is initially homogeneous, the emerging critical
 245 mode only contains the cavity fields, the homogeneous atom state and the $\pm Q$ atom modes.
 246 These modes constitute the center manifold

$$\mathbf{v}_{cm} = (\phi_0, \phi_1, \psi_0, \psi_Q, \psi_{-Q})^T. \quad (10)$$

247 The normal phase $\mathbf{X}_0 = (0, 0, 1, 0, 0)^T$ is a fixed point of F . When $\tilde{\eta} < \eta_c$ this fixed point
 248 is stable but becomes unstable for $\tilde{\eta} \geq \eta_c$.

249 As stated in the main text, slightly past the critical point the symmetry-broken state
 250 can be approximated as

$$\mathbf{u} = \sqrt{\mu} R \mathbf{v}^R e^{i\omega_c t} + c.c., \quad (11)$$

251 where $\mu = \tilde{\eta} - \eta_c$ is the absolute distance to the critical point and ω_c is the frequency of
 252 the unstable right eigenvector \mathbf{v}^R . We will write the equations of motion in terms of the
 253 real (x_α) and imaginary part (p_α) of the complex fields in which the center manifold is
 254 spanned by vectors of the form

$$\mathbf{v}^R = (\mathbf{v}_{c1}^R, \mathbf{v}_{c2}^R, \mathbf{v}_Q^R, \mathbf{v}_{-Q}^R)^T, \quad (12)$$

255 with $\mathbf{v}_\alpha^R = (x_\alpha, p_\alpha)^T$. The approximation in Eq. (11) only describes the new fixed point
 256 well if the bifurcation is of the supercritical form, which means that the self-interaction of
 257 the critical mode is repulsive. The linear coefficient in the amplitude equation Eq. (7) is
 258 given by the real part of

$$\lambda = \sum_{i,j} \mathbf{v}_i^L \left(\frac{\partial L}{\partial \mu} \right)_{i,j} \mathbf{v}_j^R, \quad (13)$$

259 where the latin indices run over all components in the center manifold $i, j \in \{x_{c1}, p_{c1}, x_{c2}$
 260 $, p_{c2}, x_Q, p_Q, x_{-Q}, p_{-Q}\}$. The Jacobian matrix $L = \nabla F|_{\mathbf{X}_0}$ evaluated at the normal-phase

261 fixed point \mathbf{X}_0 and \mathbf{v}^L (\mathbf{v}^R) is the left (right) critical eigenvector. We define the linear
 262 coefficient as $\gamma = \text{Re}(\lambda)$. The cubic coefficient of Eq. (7) is given by the real part of

$$g = -\frac{1}{2} \sum_{i,j,k,q} \mathbf{v}_i^L \frac{\partial^3 F_i}{\partial \mathbf{X}^j \partial \mathbf{X}^k \partial \mathbf{X}^q} \Big|_{\mathbf{X}_0, \mu=0} \mathbf{v}_j^R \mathbf{v}_k^R \bar{\mathbf{v}}_q^R = -\mathbf{v}_i^L (N_0)_i^{j,k,q} \mathbf{v}_j^R \mathbf{v}_k^R \bar{\mathbf{v}}_q^R, \quad (14)$$

263 where the cubic coefficient in the main text is $g^r = \text{Re}(g)$. Within the center manifold
 264 there is no contribution to quadratic contribution from $\partial^2 F$ because the center manifold
 265 obeys a reflection symmetry, which originates from the fact that the coupled Eqs. (1)
 266 and (2) posses a \mathcal{Z}_2 -symmetry. This symmetry is that the equations are invariant under the
 267 simultaneous phase shift of the atoms by $\psi_k \rightarrow e^{i\pi k/Q} \psi_k$ and the cavity fields $\phi_j \rightarrow -\phi_j$.

268 A.1 The critical eigenvector

269 To compute λ and g we use that the symmetry results in the right and left eigenvector
 270 components for each mode $\alpha \in \{c_1, c_2, Q, -Q\}$ are related by

$$\mathbf{v}_\alpha^L = \pm \sigma_x \mathbf{v}_\alpha^R, \quad (15)$$

271 where σ_x is the first Pauli spin-1/2 matrix. Furthermore, the eigenvectors are normalized
 272 such that Eq. (15) is realized with the upper sign. The two effective interaction parameters
 273 can now be written solely in terms of the right eigenvectors

$$\begin{aligned} \lambda &= \sum_{i,j} ((\mathbb{1}_4 \otimes \sigma_x) \mathbf{v}^R)_i \left(\frac{\partial L}{\partial \mu} \right)_{i,j} \mathbf{v}_j^R, \\ g &= - \sum_{i,j,k,k,q} ((\mathbb{1}_4 \otimes \sigma_x) \mathbf{v}^R)_i (N_0)_i^{j,k,q} \mathbf{v}_j^R \mathbf{v}_k^R \bar{\mathbf{v}}_q^R. \end{aligned} \quad (16)$$

274 The cavity eigenvector components are connected to the atomic eigenvector components
 275 through the definition of the critical eigenvector

$$(L_0 - i\omega_c) \mathbf{v}^R = \mathbf{0}, \quad (17)$$

276 which leads to the relation

$$\mathbf{v}_{c_j}^R = -\sqrt{2} \eta_c \beta_j \begin{pmatrix} 1 & 0 & 1 & 0 \\ \frac{\kappa+i\omega_c}{\Delta_j} & 0 & \frac{\kappa+i\omega_c}{\Delta_j} & 0 \end{pmatrix} \begin{pmatrix} x_Q \\ p_Q \\ x_{-Q} \\ p_{-Q} \end{pmatrix}, \quad (18)$$

277 where

$$\beta_j = \frac{\Delta_j}{2} \frac{\Delta_j^2 + \kappa^2 - \omega_c^2 - 2i\omega_c \kappa}{\Delta_j^4 + 2\Delta_j^2(\kappa^2 - \omega_c^2) + (\kappa^2 + \omega_c^2)^2}. \quad (19)$$

278 From the critical eigenvalue condition $\det(L_0 - I\omega_c) = 0$ one finds

$$\eta_c^2 \beta = \eta_c^2 \sum_{j=1,2} \text{Re} \beta_j = \frac{\omega_a^2 - \omega_c^2}{2E_R}, \quad (20)$$

$$\text{Im} \beta_j = 0.$$

279 Linearizing around the normal phase means that the short-range interaction only couples
 280 the modes Q and $-Q$ in a symmetric manner. As the cavity also couples identically to
 281 these two modes, the components of the critical eigenvector obeys $x_Q = x_{-Q} = x_a$ and

282 $p_Q = p_{-Q} = p_a$. Using this symmetry x_a and p_a can be connected through Eq. (17) and
 283 one finds

$$p_a = \frac{i\omega_c}{E_R} x_a = i\tilde{\omega} x_a, \quad (21)$$

284 where the dimensionless frequency $\tilde{\omega} = \omega_c/E_R$ has been introduced for later convenience.
 285 Now \mathbf{v}^R can be fully expressed through the parameters of our theory and x_a . A closed-form
 286 expression for x_a can be found through the normalization condition

$$\sum_i \mathbf{v}_i^L \mathbf{v}_i^R = 1 \rightarrow x_a = \frac{1}{2} \left(4\eta_c^2 \sum_j \left[\beta_j^2 \frac{\kappa + i\omega_c}{\Delta_j} \right] + \frac{i\omega_c}{E_R} \right)^{-1/2}. \quad (22)$$

287 This form of x_a guarantees the upper sign in Eq. (15).

288 A.2 Computing g^r and γ

289 By substituting the critical eigenvector into Eq. (13) one finds the expression

$$\begin{aligned} \lambda &= \frac{8}{\eta_c} x_a^2 \eta_c^2 \beta = \frac{2\eta_c^2 \beta}{\eta_c \left(4\eta_c^2 \sum_j \left[\beta_j^2 \frac{\kappa + i\omega_c}{\Delta_j} \right] + \frac{i\omega_c}{E_R} \right)} \\ &= \frac{\omega_a^2 - \omega_c^2}{E_R} \frac{1}{\eta_c \left(4\eta_c^2 \sum_j \left[\beta_j^2 \frac{\kappa + i\omega_c}{\Delta_j} \right] + \frac{i\omega_c}{E_R} \right)}. \end{aligned} \quad (23)$$

290 The expression for g is

$$\begin{aligned} g &= x_a^2 |x_a|^2 E^R \left(\tilde{U} (3 + 2\tilde{\omega}^2 + 3\tilde{\omega}^4) + 4(1 - \tilde{\omega}^2)(3 + \tilde{\omega}^2) \right) \\ &= x_a^2 |x_a|^2 E^R W_a(\tilde{U}, \tilde{\omega}) \end{aligned} \quad (24)$$

291 where the dimensionless interaction is defined as $\tilde{U} = U/E_R$.

292 It is clear that the only part that makes both λ and g complex is in x_a^2 . As the
 293 coefficients for our theory are related to the real part of λ and g , it is relevant to extract
 294 the real part of x_a^2

$$\begin{aligned} \text{Re}(x_a^2) &= \eta_c^2 \kappa \frac{\sum_j \frac{\beta_j^2}{\Delta_j}}{\left| \left(4\eta_c^2 \sum_j \left[\beta_j^2 \frac{\kappa + i\omega_c}{\Delta_j} \right] + \frac{i\omega_c}{E_R} \right) \right|^2} \\ &= \frac{\eta_c^2 \kappa}{2 \left| \left(4\eta_c^2 \sum_j \left[\beta_j^2 \frac{\kappa + i\omega_c}{\Delta_j} \right] + \frac{i\omega_c}{E_R} \right) \right|^2} \sum_j \Delta_j \frac{\left(\Delta_j^2 + \kappa^2 - \omega_c^2 \right)^2 + 4\omega_c^2 \left(\Delta_j^2 - \omega_c^2 \right)}{\left(\Delta_j^4 + 2\Delta_j^2 (\kappa^2 - \omega_c^2) + (\kappa^2 + \omega_c^2)^2 \right)^2}. \end{aligned} \quad (25)$$

295 This directly shows that the only dependence on U in x_a is through η_c in Eq. (4). Due
 296 to the complexity of the full closed form expression of g it is insightful to consider the
 297 behavior of $\text{Re}(x_a^2)$ and W_a separately.

298 First considering W_a

$$W_a(\tilde{U}, \tilde{\omega}) = \tilde{U} (3 + 2\tilde{\omega}^2 + 3\tilde{\omega}^4) + 4(1 - \tilde{\omega}^2)(3 + \tilde{\omega}^2). \quad (26)$$

299 The interesting feature of W_a is the fact that it has a sign change through a zero-crossing
 300 at a critical frequency $\tilde{\omega}_0$ such that $W_a(\tilde{U}, \tilde{\omega}_0) = 0$. The closed form expression for $\tilde{\omega}_0$ is

$$\tilde{\omega}_0 = \sqrt{\frac{\tilde{U} - 4 + 2\sqrt{2}\sqrt{8 - 4\tilde{U} - \tilde{U}^2}}{4 - 3\tilde{U}}} = \sqrt{1 + \frac{\tilde{U}}{2} + \mathcal{O}(\tilde{U}^2)}. \quad (27)$$

301 This exactly defines the separatrix U_{c2} shown as a black line in Fig. 1(b). Fig. 1(b) is
 302 plotted as a function of Δ and not ω_c because of the atom instability. In the regime where
 303 $\kappa < E_R$, the equations simplify because near $\Delta \sim E_R$ one has that $\omega_c \approx \Delta$. This means
 304 that one can replace $\tilde{\omega}_0$ with Δ/E_R instead of substituting in the full expression in Eq. (3).
 305 The relevant quantity that one should compare $\tilde{\omega}_0$ to is the dimensionless frequency of the
 306 bare atomic instability, which happens at

$$\tilde{\omega}_a = \sqrt{1 + 2\tilde{U}}, \quad (28)$$

307 and which sets the dashed separatrix U_{c1} in Fig. 1(b). For $\tilde{U} = 0$ the frequencies $\tilde{\omega}_0$ and
 308 $\tilde{\omega}_a$ coincide, which means that there will be no cubic interactions for the atomic instability
 309 without short-range interactions. As \tilde{U} is made finite we see from the expansion in Eq. (27)
 310 that $\tilde{\omega}_a > \tilde{\omega}_0$ for small $\tilde{U} < 1$. By keeping the full expression for $\tilde{\omega}_0$, one finds that the
 311 critical \tilde{U}_c where $\tilde{\omega}_a = \tilde{\omega}_0$ is

$$\tilde{U}_c = \sqrt{2}, \quad (29)$$

312 which is the intersection point of the separatrices at finite U with $\Delta = \sqrt{1 + 2\sqrt{2}}E_R$.
 313 Below this interaction strength, $\tilde{\omega}_0$ is smaller than $\tilde{\omega}_a$. The effect is that $W_a(\tilde{U}, \tilde{\omega}_a) < 0$
 314 for all $\tilde{U} < \tilde{U}_c$.

315 To determine the nature of the interactions one has to determine the sign of $\text{Re}(x_a^2)$.
 316 This sign is fixed by the numerator of Eq. (25) and using the parametrization discussed
 317 in the main text one finds

$$\sum_{j=1,2} \Delta_j \left((\Delta_j^2 + \kappa^2 - \omega_c^2)^2 + 4\omega_c^2 (\Delta_j^2 - \omega_c^2) \right) = \frac{\delta}{2} \left(\frac{(\delta^2 + 4\kappa^2)^2}{16} + \Delta^2 (3\delta^2 + 4\kappa^2) + 8\Delta^4 \right). \quad (30)$$

318 So for any values of κ , Δ and $|\delta|$, the sign of $\text{Re}(x_a^2)$ is set by the sign of δ . This means that
 319 for a chosen sign of δ the sign of W_a determines whether the non-linear self-interactions
 320 are repulsive or attractive. Additionally this also means that $\gamma > 0$. If $\delta > 0$ then $\omega_c < \omega_a$
 321 and both $\eta_c^2\beta$ in Eq. (20) and $\text{Re}(x_a^2)$ are greater than zero. If $\delta < 0$ then $\omega_c > \omega_a$ and
 322 both $\eta_c^2\beta$ and $\text{Re}(x_a^2)$ are negative such that γ is again positive.

323 Next consider the fraction γ/g^r which determines the magnitude of the stable time-
 324 crystalline phase. By using the above derived relations one can show that it scales with

325 $\sqrt{\epsilon}$ in the limit where $\omega_c^2 \rightarrow \omega_a^2 - \epsilon$ with $\epsilon \ll \{E_R, \Delta_{1/2}, \kappa\}$

$$\begin{aligned}
\lim_{\omega_c^2 \rightarrow \omega_a^2 - \epsilon} \frac{\gamma}{g^r} &= \lim_{\omega_c^2 \rightarrow \omega_a^2 - \epsilon} \frac{8}{\eta_c} \frac{\omega_a^2 - \omega_c^2}{2E_R} \frac{\text{Re}(x_a^2)}{\text{Re}(x_a^2) |x_a|^2 E_R W_a(U/E_R, \omega/E_R)} \\
&= \lim_{\omega_c^2 \rightarrow \omega_a^2 - \epsilon} \frac{32}{\eta_c} \frac{\omega_a^2 - \omega_c^2}{2E_R^2 W_a(U/E_R, \omega/E_R)} \left| 4\eta_c^2 \sum_j \left[\beta_j^2 \frac{\kappa + i\omega_c}{\Delta_j} \right] + \frac{i\omega_c}{E_R} \right| \\
&= \lim_{\omega_c^2 \rightarrow \omega_a^2 - \epsilon} \frac{32}{\sqrt{\frac{\omega_a^2 - \omega_c^2}{E_R \sum_{j=1,2} \frac{\Delta_j (\Delta_j^2 + \kappa^2 - \omega_c^2)}{\omega_c^4 + 2\omega_c^2 (\kappa^2 - \Delta_j^2) + (\Delta_j^2 + \kappa^2)^2}}} \frac{\omega_a^2 - \omega_c^2}{2E_R^2 W_a(U/E_R, \omega/E_R)} \\
&\quad \times \left| 4\eta_c^2 \sum_j \left[\beta_j^2 \frac{\kappa + i\omega_c}{\Delta_j} \right] + \frac{i\omega_c}{E_R} \right| \\
&= 32\sqrt{\epsilon} \frac{\sqrt{E_R \sum_{j=1,2} \frac{\Delta_j (\Delta_j^2 + \kappa^2 - \omega_a^2)}{\omega_a^4 + 2\omega_a^2 (\kappa^2 - \Delta_j^2) + (\Delta_j^2 + \kappa^2)^2}}}{2E_R^2 W_a(U/E_R, \omega/E_R)} \frac{\omega_a}{E_R} + \mathcal{O}(\epsilon^{3/2}).
\end{aligned} \tag{31}$$

326 This is important as it proves that the AI region does not possess a stable time-crystalline
327 solution, to leading order in μ , as $\epsilon \rightarrow 0$ for the AI.

328 The fact that we have analytical expressions for all the important quantities also
329 allows us to show some intriguing features of the time-crystalline phase within the center
330 manifold. The first important feature was discussed in the main text, namely that the
331 frequency of OSR phase is independent of the atom parameters. The second important
332 feature we will show now is that the time-averaged occupation in the recoil field is only
333 indirectly depending on the cavity parameters. As stated in the conclusions, this means
334 that our heating discussion is more generic, as it does not depend on the specific cavity
335 configuration. If we write Eq. (5) using x_a and p_a the occupation in the recoil mode is
336 given by

$$\begin{aligned}
|\psi_Q(t)|^2 &= \frac{1}{2} (|x_a|^2 + |p_a|^2) \\
&= \frac{\mu}{4} R^2 \left(2|x_a|^2 + x_a^2 \exp(i2\omega_c t) + \bar{x}_a^2 \exp(-i2\omega_c t) \right. \\
&\quad \left. + 2|p_a|^2 + p_a^2 \exp(i2\omega_c t) + \bar{p}_a^2 \exp(-i2\omega_c t) \right).
\end{aligned} \tag{32}$$

337 Due to the periodicity of the system the time average is given by

$$\langle |\psi_Q|^2 \rangle_T = \int_0^{2\pi/\omega_c} |\psi_Q(t)|^2 dt = \frac{\mu}{2} R^2 (|x_a|^2 + |p_a|^2) = \frac{\mu}{2} R^2 |x_a|^2 (1 + \tilde{\omega}^2), \tag{33}$$

338 where p_a have been eliminated through Eq. (21). Using the results from Eqs. (23) and (24)
339 we find

$$R^2 = \frac{\text{Re}(\lambda)}{\text{Re}(g)} = \frac{4(\tilde{\omega}_a^2 - \tilde{\omega}^2)}{\eta_c |x_a|^2 W_a(\tilde{U}, \tilde{\omega})}. \tag{34}$$

340 Inserting this into Eq. (33) we find

$$\langle |\psi_Q|^2 \rangle_T = \frac{2\eta(\tilde{\omega}_a^2 - \tilde{\omega}^2)(1 + \tilde{\omega}^2)}{W_a(\tilde{U}, \tilde{\omega})}, \tag{35}$$

341 which only depends on the atom parameters, the OSR frequency, and the relative depth
 342 into the OSR phase, η . The same $\tilde{\omega}$ can be generated with many different cavity con-
 343 figurations, for example by changing δ and having a small κ or even more generally by
 344 departing from the fully symmetric case presented here.

345 B Including fluctuations outside the center manifold

346 While our theory within the center manifold predicts that the time crystal is stable also
 347 with finite interactions U , it does not capture atom modes outside of the center manifold.
 348 The contact interaction allows occupation in the center manifold to scatter to the other
 349 atom modes with momenta different from $\pm Q$ and 0. Inside the OSR phase the NCM
 350 modes can be occupied due to the presence of the OSR. This leads to heating and poten-
 351 tially also the destruction of the time crystal in the long time limit. One way to describe
 352 this is to linearize around the OSR solution $\mathbf{v}_{\text{osr}}(t)$

$$\mathbf{v}(t) = \mathbf{v}_{\text{osr}}(t) + \delta\mathbf{v}(t). \quad (36)$$

353 This leads to an equation for the fluctuations

$$\begin{aligned} \dot{\mathbf{v}} &= \dot{\mathbf{v}}_{\text{osr}} + \delta\dot{\mathbf{v}} = F(\mathbf{v}_{\text{osr}} + \delta\mathbf{v}) = F(\mathbf{v}_{\text{osr}}) + \nabla F|_{\mathbf{v}=\mathbf{v}_{\text{osr}}} \delta\mathbf{v} + \mathcal{O}(\delta\mathbf{v}^2) \\ &\rightarrow \delta\dot{\mathbf{v}} = \nabla F|_{\mathbf{v}=\mathbf{v}_{\text{osr}}} \delta\mathbf{v} + \mathcal{O}(\delta\mathbf{v}^2) \approx J_{\text{osr}}(t)\delta\mathbf{v}, \end{aligned} \quad (37)$$

354 where $J_{\text{osr}}(t)$ is a time-dependent matrix-valued function. Using the approximate fixed
 355 point from the analytical OSR solution we can derive an approximate form of $J_{\text{osr}}(t)$. Due
 356 to the periodicity of the OSR solution $J_{\text{osr}}(t)$ can be expanded in a discrete Fourier series
 357 of the form

$$J_{\text{osr}}(t) = \sum_{n=-4}^4 M_n e^{in\omega_c t}. \quad (38)$$

358 The coupling to the cavity in Eq. (1) is proportional to a product of a NCM mode and
 359 a cavity field. To first order in fluctuations there is therefore no coupling between cavity
 360 fluctuations and the NCM modes. For the leading-order heating mechanism $\delta\mathbf{v}$ only
 361 includes the atom modes with momentum $k \notin \{0, Q, -Q\}$ and is therefore solely described
 362 by Eq. (1) with the cavity fields replaced by the OSR solution. It is for this reason that
 363 we are able to use the simple scattering description, discussed in the main text, to predict
 364 the momentum of the growing modes.

365 Because the cavity loss has already been used to stabilize the OSR phase within the
 366 center manifold this means that the cavity is not able to cool down the NCM modes
 367 at the linear level. As one includes higher orders in fluctuations the cavity fluctuations
 368 can potentially start cooling down the NCM but as this is a higher-order effect, fine
 369 tuning would be needed to make it overcome the first-order heating before the system has
 370 thermalized and the OSR phase is destroyed.

371 To verify our simple scattering predictions we derive $J_{\text{osr}}(t)$ from Eq. (1). The linearized
 372 equation for the NCM mode with momentum k is

$$\begin{aligned} i\partial_t \psi_k &= \left(-\dot{\Omega} + k^2 - U|\hat{\psi}_0|^2 + 2U \left(|\hat{\psi}_0|^2 + |\hat{\psi}_Q|^2 + |\hat{\psi}_{-Q}|^2 \right) \right) \psi_k + U \left(\hat{\psi}_0^2 + 2\hat{\psi}_{-Q}\psi_Q \right) \tilde{\psi}_{-k} \\ &\quad + \frac{\tilde{\eta}}{\sqrt{2}} \sum_j \text{Re}(\hat{\psi}_j) (\psi_{k+Q} + \psi_{k-Q}), \end{aligned} \quad (39)$$

373 where the hat has been used to identify the OSR components that are approximated as
 374 unchanged within the linearization. The overall phase of the atoms is set by $\hat{\Omega}$ and chosen
 375 such that $\text{Im}\{\psi_0\} = 0$ within the center manifold [24]. Within the linearization the value
 376 is

$$\begin{aligned}
 \hat{\Omega} = & \frac{\tilde{\eta}}{\sqrt{2}} \sum_j \text{Re}(\phi_j) \frac{\psi_Q + \bar{\psi}_Q + \psi_{-Q} + \bar{\psi}_{-Q}}{2\psi_0} \\
 & + U \left(2 - \psi_0^2 + \frac{1}{2} [(\psi_Q + \bar{\psi}_Q)(\psi_{-Q} + \bar{\psi}_{-Q}) + (\psi_Q - \bar{\psi}_Q)(\psi_{-Q} - \bar{\psi}_{-Q})] \right).
 \end{aligned} \tag{40}$$

377 From Eq. (39) we see that the finite occupation of the cavity field leads to coupling of
 378 the k NCM mode with the NCM mode at $k \pm Q$. As the occupation of the NCM fields
 379 are small and we consider $\omega_c < E_R$, one can truncate after one recoil kick such that
 380 $|k| < Q$. This is confirmed by the full numerical solution of Eqs. (1) and (2) shown in
 381 the main text. With this truncation each NCM, ψ_k , couples to the seven other fields
 382 $\{\bar{\psi}_k, \psi_{-k}, \bar{\psi}_{-k}, \psi_{k-Q}, \bar{\psi}_{k-Q}, \psi_{-k+Q}, \bar{\psi}_{-k+Q}\}$. For each value of k we therefore find a
 383 $J_{\text{OSR}}(t)$ given by

$$J_{\text{OSR}}(t) = i \begin{pmatrix} -m_k & 0 & 0 & -g_k & -m_Q & -g_Q & 0 & 0 \\ 0 & \bar{m}_k & \bar{g}_k & 0 & \bar{g}_Q & \bar{m}_Q & 0 & 0 \\ 0 & -g_k & -m_k & 0 & 0 & 0 & -m_Q & -g_Q \\ \bar{g}_k & 0 & 0 & \bar{m}_k & 0 & 0 & \bar{g}_Q & \bar{m}_Q \\ -m_Q & -g_Q & 0 & 0 & -m_{k-Q} & 0 & 0 & -g_k \\ \bar{g}_Q & \bar{m}_Q & 0 & 0 & 0 & \bar{m}_{k-Q} & \bar{g}_k & 0 \\ 0 & 0 & -m_Q & -g_Q & 0 & -g_k & -m_{k-Q} & 0 \\ 0 & 0 & \bar{g}_Q & \bar{m}_Q & \bar{g}_k & 0 & 0 & \bar{m}_{k-Q} \end{pmatrix}, \tag{41}$$

384 with the vector $\delta \mathbf{v}^T = (\psi_k, \bar{\psi}_k, \psi_{-k}, \bar{\psi}_{-k}, \psi_{k-Q}, \bar{\psi}_{k-Q}, \psi_{-k+Q}, \bar{\psi}_{-k+Q})^T$ and the five
 385 different entries being

$$\begin{aligned}
 m_k &= k^2 + U - 2U \left(\hat{\psi}_Q^2 + \hat{\psi}_Q^2 \right) - \frac{\tilde{\eta}}{\sqrt{2}} \sum_j \text{Re}(\hat{\phi}_j) \frac{\hat{\psi}_Q + \hat{\psi}_Q}{\hat{\psi}_0}, \\
 m_{k-Q} &= m_{k \rightarrow k-Q}, \\
 m_Q &= \frac{\tilde{\eta}}{\sqrt{2}} \sum_j \text{Re}(\hat{\phi}_j) + 2U \hat{\psi}_0 \left(\hat{\psi}_Q + \hat{\psi}_Q \right), \\
 g_k &= U \left(2\hat{\psi}_Q^2 + \hat{\psi}_0^2 \right), \\
 g_Q &= 2U \hat{\psi}_Q \hat{\psi}_0.
 \end{aligned} \tag{42}$$

386 Inserting the OSR solutions into Eq. (42) one finds an analytical expression for $J_{\text{OSR}}(t)$
 387 which is periodic such that $J_{\text{OSR}}(t) = J_{\text{OSR}}(t + T)$ with $T = 2\pi/\omega_c$. We then employ
 388 standard Floquet theory by numerically time-evolving the eight equations over one period
 389 T . This allows us to find the fundamental matrix $\Phi(t)$ which is defined as the solution to

$$\partial_t \Phi(t) = J_{\text{OSR}}(t) \Phi(t), \tag{43}$$

390 with the initial condition $\Phi(0) = \mathbf{1}_8$. The eigenvalues λ_i of the monodromy matrix $M =$
 391 $\Phi(T)$ determines the growth rates of the NCM modes $\Gamma_i = \text{Re}(\log(\lambda_i)/T)$. To understand
 392 the initial heating effects we only need to investigate the eigenmode with the largest growth
 393 rate $\Gamma = \max(\Gamma_i)$. By Computing Γ as a function of k we are able to compute the growth
 394 rates of the different channels as plotted in Fig. 3.

References

- 395
- 396 [1] F. Wilczek, *Quantum time crystals*, Phys. Rev. Lett. **109**, 160401 (2012),
397 doi:10.1103/PhysRevLett.109.160401.
- 398 [2] A. Shapere and F. Wilczek, *Classical time crystals*, Phys. Rev. Lett. **109**, 160402
399 (2012), doi:10.1103/PhysRevLett.109.160402.
- 400 [3] P. Nozières, *Time crystals: Can diamagnetic currents drive a charge density*
401 *wave into rotation?*, Europhysics Letters **103**(5), 57008 (2013), doi:10.1209/0295-
402 5075/103/57008.
- 403 [4] P. Bruno, *Impossibility of spontaneously rotating time crystals: A no-go theorem*,
404 Phys. Rev. Lett. **111**, 070402 (2013), doi:10.1103/PhysRevLett.111.070402.
- 405 [5] H. Watanabe and M. Oshikawa, *Absence of quantum time crystals*, Phys. Rev. Lett.
406 **114**, 251603 (2015), doi:10.1103/PhysRevLett.114.251603.
- 407 [6] J. Zhang, P. W. Hess, A. Kyprianidis, P. Becker, A. Lee, J. Smith, G. Pagano, I.-D.
408 Potirniche, A. C. Potter, A. Vishwanath, N. Y. Yao and C. Monroe, *Observation of*
409 *a discrete time crystal*, Nature **543**(7644), 217 (2017), doi:10.1038/nature21413.
- 410 [7] S. Choi, J. Choi, R. Landig, G. Kucsko, H. Zhou, J. Isoya, F. Jelezko, S. Onoda,
411 H. Sumiya, V. Khemani, C. von Keyserlingk, N. Y. Yao *et al.*, *Observation of discrete*
412 *time-crystalline order in a disordered dipolar many-body system*, Nature **543**(7644),
413 221 (2017), doi:10.1038/nature21426.
- 414 [8] J. Rovny, R. L. Blum and S. E. Barrett, *Observation of discrete-time-crystal signa-*
415 *tures in an ordered dipolar many-body system*, Phys. Rev. Lett. **120**, 180603 (2018),
416 doi:10.1103/PhysRevLett.120.180603.
- 417 [9] S. Pal, N. Nishad, T. S. Mahesh and G. J. Sreejith, *Temporal order in period-*
418 *ically driven spins in star-shaped clusters*, Phys. Rev. Lett. **120**, 180602 (2018),
419 doi:10.1103/PhysRevLett.120.180602.
- 420 [10] J. Randall, C. Bradley, F. van der Gronden, A. Galicia, M. Abobeih, M. Markham,
421 D. Twitchen, F. Machado, N. Yao and T. Taminiau, *Many-body-localized discrete*
422 *time crystal with a programmable spin-based quantum simulator*, Science **374**(6574),
423 1474 (2021).
- 424 [11] X. Mi, M. Ippoliti, C. Quintana, A. Greene, Z. Chen, J. Gross, F. Arute, K. Arya,
425 J. Atalaya, R. Babbush *et al.*, *Time-crystalline eigenstate order on a quantum pro-*
426 *cessor*, Nature **601**(7894), 531 (2022).
- 427 [12] H. Keßler, P. Kongkhambut, C. Georges, L. Mathey, J. G. Cosme and A. Hem-
428 merich, *Observation of a dissipative time crystal*, Phys. Rev. Lett. **127**, 043602
429 (2021), doi:10.1103/PhysRevLett.127.043602.
- 430 [13] H. Taheri, A. B. Matsko, L. Maleki and K. Sacha, *All-optical dissipative discrete time*
431 *crystals*, Nature communications **13**(1), 848 (2022).
- 432 [14] P. Kongkhambut, J. Skulte, L. Mathey, J. G. Cosme, A. Hemmerich and
433 H. Keßler, *Observation of a continuous time crystal*, Science **377**(6606), 670
434 (2022), doi:10.1126/science.abo3382, [https://www.science.org/doi/pdf/10.](https://www.science.org/doi/pdf/10.1126/science.abo3382)
435 [1126/science.abo3382](https://www.science.org/doi/pdf/10.1126/science.abo3382).

- 436 [15] D. Dreon, A. Baumgärtner, X. Li, S. Hertlein, T. Esslinger and T. Donner, *Self-*
437 *oscillating pump in a topological dissipative atom-cavity system*, Nature **608**(7923),
438 494 (2022), doi:10.1038/s41586-022-04970-0.
- 439 [16] X. Li, D. Dreon, P. Zupancic, A. Baumgärtner, A. Morales, W. Zheng, N. R.
440 Cooper, T. Donner and T. Esslinger, *First order phase transition between two*
441 *centro-symmetric superradiant crystals*, Phys. Rev. Res. **3**, L012024 (2021),
442 doi:10.1103/PhysRevResearch.3.L012024.
- 443 [17] F. Piazza and P. Strack, *Quantum kinetics of ultracold fermions coupled to an optical*
444 *resonator*, Physical Review A **90**(4), 043823 (2014).
- 445 [18] S. Schütz and G. Morigi, *Prethermalization of atoms due to photon-mediated long-*
446 *range interactions*, Physical review letters **113**(20), 203002 (2014).
- 447 [19] F. Mivehvar, F. Piazza, T. Donner and H. Ritsch, *Cavity qed with quantum*
448 *gases: new paradigms in many-body physics*, Advances in Physics **70**(1), 1 (2021),
449 doi:10.1080/00018732.2021.1969727, [https://doi.org/10.1080/00018732.2021.](https://doi.org/10.1080/00018732.2021.1969727)
450 [1969727](https://doi.org/10.1080/00018732.2021.1969727).
- 451 [20] C. H. Johansen, J. Lang, A. Morales, A. Baumgärtner, T. Donner and F. Piazza,
452 *Multimode-polariton superradiance via floquet engineering*, SciPost Physics **12** (2022),
453 doi:10.21468/SciPostPhys.12.3.094.
- 454 [21] H. Keßler, J. Klinder, M. Wolke and A. Hemmerich, *Optomechanical atom-cavity*
455 *interaction in the sub-recoil regime*, New Journal of Physics **16**(5), 053008 (2014),
456 doi:10.1088/1367-2630/16/5/053008.
- 457 [22] P. Domokos and H. Ritsch, *Collective cooling and self-organization of atoms in a*
458 *cavity*, Phys. Rev. Lett. **89**, 253003 (2002), doi:10.1103/PhysRevLett.89.253003.
- 459 [23] K. Baumann, C. Guerlin, F. Brennecke and T. Esslinger, *Dicke quantum phase*
460 *transition with a superfluid gas in an optical cavity*, Nature **464**, 1301 (2010),
461 doi:10.1038/nature09009.
- 462 [24] C. H. Johansen, *Field theory of interacting polaritons under drive and dissipation*,
463 Ph.D. thesis, Technische Universität Dresden, Chap. 4 (2023).
- 464 [25] J. del Pino, J. Kořata and O. Zilberberg, *Limit cycles as stationary states of an*
465 *extended harmonic balance ansatz*, arXiv preprint arXiv:2308.06092 (2023).
- 466 [26] A. Kosior, H. Ritsch and F. Mivehvar, *Nonequilibrium phases of ultracold bosons with*
467 *cavity-induced dynamic gauge fields*, arXiv **89** (2022), doi:10.48550/arXiv.2208.04602.
- 468 [27] Y. Kuramoto, *Chemical oscillations, waves, and turbulence*, Springer (1984).
- 469 [28] Y. A. Kuznetsov, *Elements of Applied Bifurcation Theory*, Springer (1998).
- 470 [29] F. Piazza and H. Ritsch, *Self-ordered limit cycles, chaos, and phase slippage with a*
471 *superfluid inside an optical resonator*, Physical review letters **115**(16), 163601 (2015).
- 472 [30] F. Gambetta, F. Carollo, M. Marcuzzi, J. Garrahan and I. Lesanovsky, *Discrete time*
473 *crystals in the absence of manifest symmetries or disorder in open quantum systems*,
474 Physical review letters **122**(1), 015701 (2019).
- 475 [31] A. Lazarides, S. Roy, F. Piazza and R. Moessner, *Time crystallinity in dissipative*
476 *floquet systems*, Physical Review Research **2**(2), 022002(R) (2020).

- 477 [32] R. Chitra and O. Zilberberg, *Dynamical many-body phases of the paramet-*
478 *rically driven, dissipative dicke model*, Phys. Rev. A **92**, 023815 (2015),
479 doi:10.1103/PhysRevA.92.023815.
- 480 [33] B. Zhu, J. Marino, N. Y. Yao, M. D. Lukin and E. A. Demler, *Dicke time crystals in*
481 *driven-dissipative quantum many-body systems*, New Journal of Physics **21**(7), 073028
482 (2019), doi:10.1088/1367-2630/ab2afe.
- 483 [34] S. A. Weidinger and M. Knap, *Floquet prethermalization and regimes of heating*
484 *in a periodically driven, interacting quantum system*, Scientific Reports **7**(1), 45382
485 (2017), doi:10.1038/srep45382.
- 486 [35] P. Mognini, L. Papariello, A. U. J. Lode and R. Chitra, *Superlattice switching from*
487 *parametric instabilities in a driven-dissipative bose-einstein condensate in a cavity*,
488 Phys. Rev. A **98**, 053620 (2018), doi:10.1103/PhysRevA.98.053620.
- 489 [36] R. J. L. Tuquero, J. Skulte, L. Mathey and J. G. Cosme, *Dissipative time crystal in*
490 *an atom-cavity system: Influence of trap and competing interactions*, Phys. Rev. A
491 **105**, 043311 (2022), doi:10.1103/PhysRevA.105.043311.
- 492 [37] L. Kofman, A. Linde and A. A. Starobinsky, *Reheating after inflation*, Phys. Rev.
493 Lett. **73**, 3195 (1994), doi:10.1103/PhysRevLett.73.3195.
- 494 [38] S. Y. Khlebnikov and I. I. Tkachev, *Classical decay of the inflaton*, Phys. Rev. Lett.
495 **77**, 219 (1996), doi:10.1103/PhysRevLett.77.219.
- 496 [39] L. Kofman, *Preheating after inflation*, Lect. Notes Phys. **738**, 55 (2008),
497 doi:10.1007/978-3-540-74353-8_2.
- 498 [40] D. Boyanovsky, H. J. de Vega, R. Holman and J. F. J. Salgado, *Analytic*
499 *and numerical study of preheating dynamics*, Phys. Rev. D **54**, 7570 (1996),
500 doi:10.1103/PhysRevD.54.7570.
- 501 [41] R. Micha and I. I. Tkachev, *Relativistic turbulence: A long way from preheating to*
502 *equilibrium*, Phys. Rev. Lett. **90**, 121301 (2003), doi:10.1103/PhysRevLett.90.121301.
- 503 [42] J. Lang and F. Piazza, *Critical relaxation with overdamped quasiparticles in open*
504 *quantum systems*, Physical Review A **94**(3), 033628 (2016).
- 505 [43] J. Lang, D. E. Chang and F. Piazza, *Nonequilibrium diagrammatic approach to*
506 *strongly interacting photons*, Physical Review A **102**(3), 033720 (2020).